AUTOMATED RENDEZVOUS AND DOCKING USING TETHERED FORMATION FLIGHT

Rebecca C. Foust*, Yashwanth K. Nakka†, Ayush Saxena‡, Soon-Jo Chung§, and Fred Y. Hadaegh¶

This paper analyzes capture strategies for tether-based autonomous rendezvous and docking. Once both spacecrafts are connected by tethers, docking is achieved through the use of reaction wheels and tether motors without the use of propellant. Autonomous rendezvous and docking is crucial for many upcoming missions including on-orbit servicing and potential Mars missions. The tether-based capture strategies investigated are a spin-up tether deployment and a free-flying child spacecraft attaching the tether. These strategies are compared to a traditional two-agent propulsive docking strategy. The capture strategies are simulated from initial orbit through to completed dock, with the total fuel consumption and dock time compared, along with initial pointing/location requirements. In addition to having lower fuel cost, the tether-based strategies are also more reliable due to redundancy, since tethers can be reeled back in and multiple tethers can be stored for use in case of primary tether failure.

INTRODUCTION

Currently, autonomous rendezvous and docking (AR&D) technologies are in high demand in low earth and low lunar orbit to support on-orbit refueling and servicing, as well as future Mars missions which will benefit from combining payloads from multiple launches to boost into Mars orbit efficiently as shown in Fig 1. AR&D has very stringent requirements and the technology is often fraught with mechanism failures, making it one of the highest risk space operations.[1] Current AR&D methods also lead to extensive fuel consumption. Careful trajectory planning and improved sensors can reduce the fuel cost somewhat, but docking by definition is the controlled collision of two satellites and as such, the failure of any subsystem can easily lead to mission failure. For example, the DART mission was intended to show the rendezvous and docking of two satellites, but instead ended in mission failure when a relatively small navigation error led to excessive fuel consumption and collision with the docking target.[2]

Performing proximity operations and docking with nanosatellites and CubeSats is particularly difficult. Nanosatellite-scale sensors and actuators are generally inaccurate and with few options, limited by availability, space, and power consumption.[3] For example, the CanX4-5 mission was able to achieve formation flying with centimeter-level position knowledge and sub-meter level control.[4] This is very successful for CubeSat missions, but for docking missions it is simply insufficient.

*Graduate Student, Aerospace Engineering, University of Illinois at Urbana-Champaign, Urbana, IL, 61801, USA
†Graduate Student, GALCIT, California Institute of Technology, Pasadena, CA, 91125, USA
‡Research Engineer, GALCIT, California Institute of Technology, Pasadena, CA, 91125, USA
§Associate Professor of Aerospace, California Institute of Technology, Pasadena, CA, 91125, USA
¶Senior Research Scientist and Chief Technologist, Jet Propulsion Laboratory, California Institute of Technology, Pasadena, CA, 91109, USA

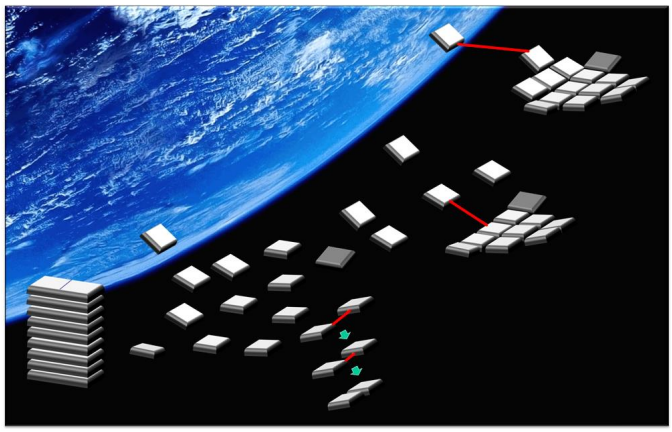

Figure 1. Concept Mission Application for Tethered Formation Flying-based AR&D

Tethered satellite docking drastically can reduce the risks associated with collision since the element colliding with the target spacecraft is much smaller than the docking target. It also avoids several other risk sources like thruster plume impingement, and fuel depletion.[1] Plume impingement can cause disturbance forces, undue heating, and particle contamination on the target.[5] This docking method can also reduce the risk of docking failure since the tether can be reeled back in and re-deployed in case of a miss, and to safeguard against drastic failures multiple backups can be brought for each mission since they are relatively lightweight. Tether-based docking is more like berthing than docking, the chaser spacecraft stays at a specified distance from the target while a controlled external element carefully connects them. Once the satellites are tethered, the final docking maneuver can be perform without expending propellant through the use of reaction wheels and tether motors. Additionally, the motor sensors can be used as a kind of relative navigation sensor. Relative navigation sensors are crucial for AR&D and are at a low TRL compared to other necessary technologies, which increases the risk of the overall mission.[6] For instance, vision-based sensors depend heavily on lighting conditions and have limited peak operational ranges. The tether motor sensors would not have these concerns and could drastically improve the relative navigation accuracy as shown by the SPHERES mission.[7,8]

Several other studies have looked into controlling tethered satellites for various missions like tethered formation flight and power generation through an electromagentic tether.[9,10] Many of these mission concepts begin with the elements already tethered. In tethered docking missions in literature, most commonly the tethers are shot out from the vehicle and left uncontrolled to intercept the chaser. Some missions propose an electromagnetic tether end-effector, which can aide in capture.[11] One such setup was tested in microgravity and achieved reasonable capture success, though it was still quite sensitive to alignment.[12] This is an excellent approach, but could be problematic in a multi-agent scenario.

This paper will demonstrate the benefits of tethered formation flight-based autonomous docking over traditional propulsive docking by leveraging the propellant-free docking actuation and analyzing two tether capture strategies. The focus of this paper is the capture phase, though the rest of the phases are included in the simulation. To accomplish this task, an accurate model of a two-spacecraft tethering system was created, which can capture the pendulum and compound pendulum modes. It has been shown previously that these modes can be fully controlled by an internal reaction

wheel assembly.[8,7,13,14] The docking operation of the spacecraft is performed by the tether motor.

Mission Overview

For this mission, the chaser vehicle performs all the maneuvering for docking with a target vehicle located at the origin of the LVLH frame. Both the chaser and the target are 30 cm cubes with a mass of 10 kg, and are assumed to be launched in the same vehicle to a 500 km orbit, so the chaser vehicle begins within a 1 km sphere around the target due to delay in separation and drift. For the tether simulations, a child spacecraft/mass is attached by the tether to the chaser. The child is a 3 cm cube weighing 0.5 kg. The tether length is restricted to 10 m though longer tethers can be used. The tether length was chosen because of the multi-agent nature of the desired mission. With multiple satellites in close range or even docking simultaneously, long tethers are a liability. This system allows for easy satellite replacement or addition to the tether-connected system. If a satellite is being replaced, it releases the tethers holding it to the others, then moves away. The new agent then moves into position and the other spacecraft release tethers to dock with it.

Nanosatellite-scale thruster options are extremely limited, but the child spacecraft could make use of a modified version of the VACCO 0.14U thruster with 5.4 mN thrust and 70 second I_{sp}.[15] The same thruster system is available at multiple scales so these parameters are also used for the parent.

The mission begins with a 1 km separation between the two satellites. At this point the initial proximity maneuver begins and places the chaser into the desired berthing maneuver position. The berthing maneuver is then performed using either thrusters or the tether, with some docking mechanism making the final rigid connection. The satellites used will be referred to as target(T), parent(P) and child(C) in figures.

INITIAL PROXIMITY MANEUVER

Traditional docking strategies focus on approaching the target using the radial or velocity directions, R-bar and V-bar respectively, or using the glideslope algorithm which merges the two while maintaining a line of sight to the target. The glideslope algorithm is typically preferred because it achieves good terminal relative velocities while staying within line of sight of the docking port, however it does perform several unoptimized burns so it can be quite expensive. Optimized versions of the glideslope algorithm exist, and achieve a great reduction in fuel cost, but they typically have worse performance on other docking constraints like a higher terminal velocity.[16] In this paper we will use the glideslope algorithm as proposed by Hablani et al. to maintain vehicle safety through a low terminal velocity.[17]

The glideslope algorithm is based on the Hill-Clohessy-Wiltshire (HCW) equations shown in Equation 1, which are a set of dynamic equations describing the relative motion of satellites in a circular orbit near to each other in the Local Vertical/Local Horizontal (LVLH) frame. The HCW equations depend only on initial state, orbit angular frequency ω, and time and are only accurate within about 30 km of the origin of the frame due to the linearization.[5] The definition for the LVLH frame can be found in Figure 2. Equation 12 shows a simplified notation for Equation 1.

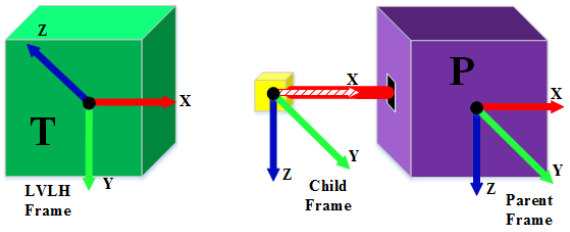

Figure 2. The frame conventions for the child and parent spacecraft

$$\begin{bmatrix} x(t) \\ y(t) \\ z(t) \\ \dot{x}(t) \\ \dot{y}(t) \\ \dot{z}(t) \end{bmatrix} = \begin{bmatrix} 1 & 0 & 6(\omega t - \sin(\omega t)) & \frac{4}{\omega}\sin(\omega t) - 3t & 0 & \frac{2}{\omega}(1-\cos(\omega t)) \\ 0 & \cos(\omega t) & 0 & 0 & \frac{\sin(\omega t)}{\omega} & 0 \\ 0 & 0 & 4 - 3\cos(\omega t) & -\frac{2}{\omega}(1-\cos(\omega t)) & 0 & \frac{\sin(\omega t)}{\omega} \\ 0 & 0 & 6\omega(1-\cos(\omega t)) & -3 + 4\cos(\omega t) & 0 & 2\sin(\omega t) \\ 0 & -\omega\sin(\omega t) & 0 & 0 & \cos(\omega t) & 0 \\ 0 & 0 & 3\omega\sin(\omega t) & -2\sin(\omega t) & 0 & \cos(\omega t) \end{bmatrix} \begin{bmatrix} x_0 \\ y_0 \\ z_0 \\ \dot{x}_0 \\ \dot{y}_0 \\ \dot{z}_0 \end{bmatrix} \tag{1}$$

$$\left[\begin{array}{c} r(t) \\ \hline v(t) \end{array}\right] = \left[\begin{array}{c|c} \Phi_{rr}(t) & \Phi_{rv}(t) \\ \hline \Phi_{vr}(t) & \Phi_{vv}(t) \end{array}\right] \left[\begin{array}{c} r_0 \\ \hline v_0 \end{array}\right] \tag{2}$$

The goal of the glideslope algorithm is to approximate a straight-line path, ρ, to the target using a chosen number of impulsive burns while satisfying line-of-sight constraints and minimizing burns near the target to reduce plume impingement. This version of the algorithm can find a trajectory even for initial and terminal positions in different planes. Thrusts performed are assumed to be impulsive and the range rate is assumed to be linearly related to the range, though this is nonlinear for close maneuvers.

First we find the vector u_0 as a function of the position at $t = 0$ and $t = T$, the terminal time.

$$u_0 = \frac{1}{\rho_0} \begin{bmatrix} x_0 \\ y_0 \\ z_0 \end{bmatrix} - \begin{bmatrix} x_T \\ y_T \\ z_T \end{bmatrix} \tag{3}$$

The XYZ position along the desired vector can be found by multiplying u_0 by the range over time. To find the range over time, we assume the range rate $\dot{\rho}$ is linearly related to the range with slope m, making the range rate equation:

$$\dot{\rho} = m\rho + \dot{\rho}_T \tag{4}$$

where $\dot{\rho}_T$ is the desired arrival speed and m can be found using this and the initial speed.

$$m = \frac{\dot{\rho}_0 - \dot{\rho}_T}{\rho_0} \tag{5}$$

Solving these equations yields an equation for range over time:

$$\rho(t) = \rho_0 e^(mt) + (\frac{\dot{\rho}_T}{m})(e^(mt) - 1) \tag{6}$$

with total transfer time, T:

$$T = \frac{1}{m} \ln(\frac{\dot{\rho}_T}{\dot{\rho}_0}) \tag{7}$$

To ensure safety, the arrival speed is chosen to be much less than the initial speed. The actual glideslope trajectory is found by performing a user-selected N burns with initial and final points along ρ. The burns are separated by $\Delta t = \frac{T}{N}$ seconds with each burn time denoted as t_b. The range of each burn $\rho_b = \rho(t_b)$ is used to calculate the XYZ position of each burn, r_b:

$$r_b = r_T + \rho_b u_0 \tag{8}$$

The ΔV expended along this trajectory can be found by leveraging the HCW equations to find the change in velocity needed to get from one r_b to the next. The $+$ superscript denotes velocity after a burn and the $-$ superscript denotes velocity before a burn.

$$v_b^+ = \Phi_{rv}^{-1}(\Delta t)(r_{b+1} - \Phi_{rr}(\Delta t) r_b) \tag{9}$$

$$v_{b+1}^- = \Phi_{vr}(\Delta t) r_b + \Phi_{vv}(\Delta t) v_b^+ \tag{10}$$

The total ΔV is then found by:

$$\Delta V = \sum_{b=1}^{N} \Phi_{rv}^{-1}(\Delta t)(r_{b+1} - \Phi_{rr}(\Delta t) r_b) - \Phi_{vr}(\Delta t) r_{b-1} + \Phi_{vv}(\Delta t) v_{b-1}^+ \tag{11}$$

where v_0^+ is simply v_0 and the position and velocity at any point along this trajectory are found by concatenating the position and velocities found using the HCW equations for each thruster firing:

$$\left[\begin{array}{c} r_b(t-t_b) \\ \hline v_b(t-t_b) \end{array}\right] = \left[\begin{array}{c|c} \Phi_{rr}(t-t_b) & \Phi_{rv}(t-t_b) \\ \hline \Phi_{vr}(t-t_b) & \Phi_{vv}(t-t_b) \end{array}\right] \left[\begin{array}{c} r_{b-1} \\ \hline v_{b-1}^+ \end{array}\right] \tag{12}$$

The free variables in this algorithm are $\dot{\rho}_0$, $\dot{\rho}_T$, N, and x_f assuming the initial position and velocity are randomly generated within the aforementioned bounds. More thruster firings leads to a lower ΔV, but increases the probability of a thruster-related failure, like a stuck open valve or over/under actuation. For this simulation, we use an initial relative speed of 30 m/s and a desired terminal relative speed of 0.1 m/s, with 3 thruster firings. The final position is 10 m in the -X direction from the target spacecraft. The result of the glideslope algorithm is shown in Figure 3. The maneuver had a total ΔV of 38.9 m/s and a total elapsed time of 188.8 seconds. The final velocity overshot the desired final speed at $[0.30, 0, -0.02]$ m/s. This can either be cleaned up with another burn at the final position or rolled in to the next step of the process. Here we elect to use this residual velocity as the initial velocity for the next phase. Using the Tsiolkovsky rocket equation,[18] we can determine the propellant mass required for this maneuver:

$$M_p = M_0(e^{\frac{\Delta V}{I_{sp} g_0}} - 1) \tag{13}$$

For the thruster parameters and spacecraft parameters chosen above, the required fuel mass is 612 g. This seems small, but this is already more than half of the propellant available to the largest thruster of the chosen type and it does not account for drift corrections, station-keeping, momentum dumps, etc.

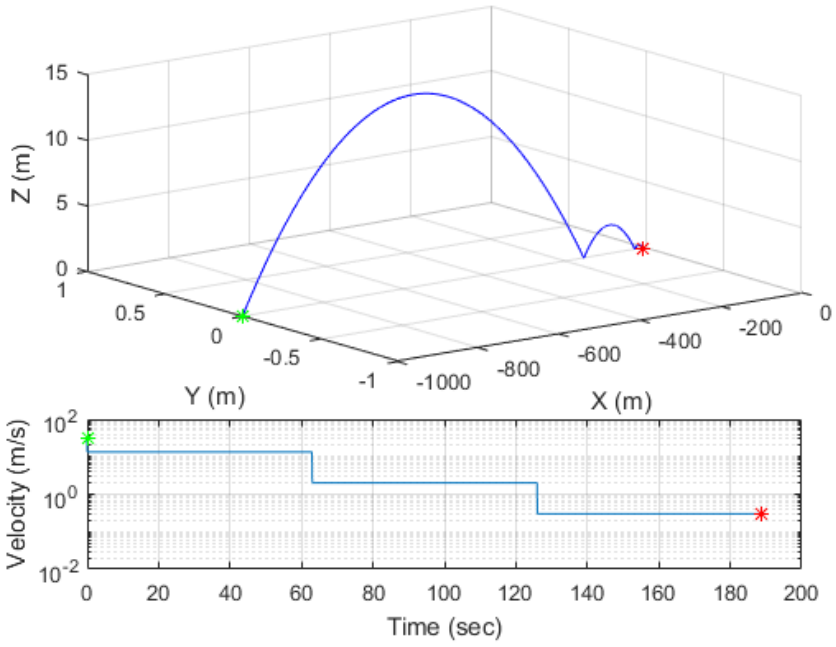

Figure 3. The glideslope approach trajectory for the parent spacecraft approaching the berthing position

BERTHING MANEUVER

The target and the parent are now separated by 10 m in the -X direction, with the parent behind the target. The final approach phase is modeled as propulsive, child-based tethered, and spin-based tethered docking.

Propulsive Docking

The propulsive docking maneuver is done using the same glideslope algorithm as the initial proximity maneuver. For this version, the initial relative speed was 0.3 m/s and the desired final speed was 0.1 mm/s, using 3 burns. The glideslope trajectory can be seen in Figure 4 The maneuver had a total ΔV of 0.30 m/s and a total elapsed time of 266.4 seconds. The final velocity was $[0.5, 0, -0.05]$ mm/s which overshot the desired final speed again. This is why the desired final speed was set so low, this overshoot cannot be cleaned up with a burn at the final time. The last burn performed occurs only 4 cm away from the target spacecraft which is highly undesirable but the speed at this location is still 7 mm/s. Depending on the capabilities of the capture mechanism, this speed may be acceptable in which case the final burn would be canceled. The fuel mass for this maneuver is 4.4 g.

Tethered Docking

When AR&D begins, the parent spacecraft expels the child spacecraft connected to the parent via the tether. The child spacecraft has a varying amount of position and attitude control, subject to study. To simplify the modeling, the tether is assumed to be in tension for the duration of the mission, which allows it to be modeled as a linear actuator with two angular degrees of freedom at

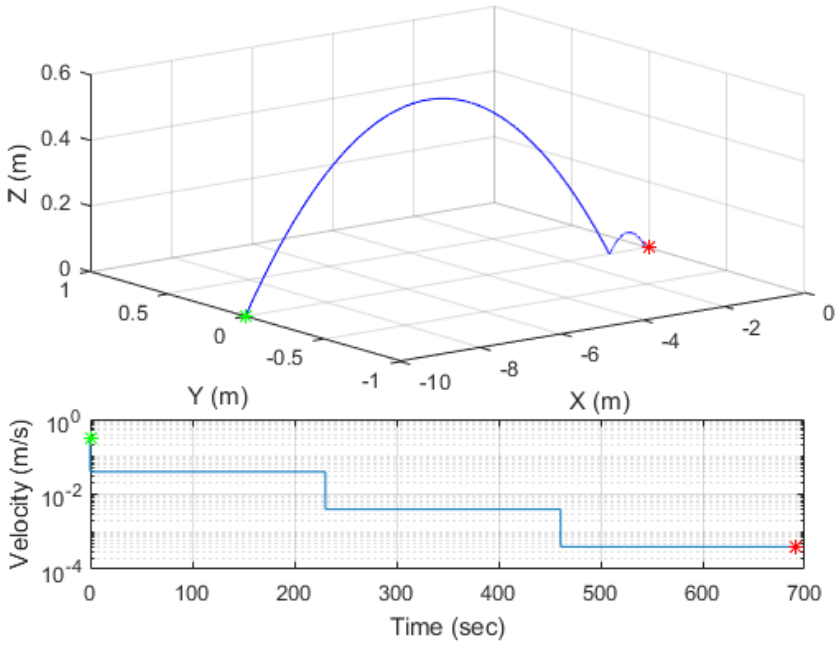

Figure 4. The glideslope approach trajectory for the child spacecraft approaching the target spacecraft's position

the base. The software model of the system was generated using SD/FAST, a robotics tool to derive the nonlinear equations of motion for a system made of pre-specified joints. The frames used in SD/FAST are shown in Figure 2. A 6DOF joint connects the parent frame to the LVLH frame.A universal joint attached to a slider joint acts as the tether connecting the child to the parent. The universal joint rotates about the parent body y and z frames. When the child spacecraft collides and attaches with the target spacecraft the change in linear momentum is significantly smaller than that of traditional docking, because the child spacecraft is much lower mass than the target spacecraft. This scheme also reduces the risk of mission failure due to docking because the parent spacecraft could have several sets of tethers and masses in case of failure.

Two capture strategies are considered for this scheme, one where the child spacecraft has full maneuverability and one where the child spacecraft is unactuated. These strategies are illustrated in Figs. 5 and 6. The two strategies greatly affect the capture mechanism used on the target spacecraft.

Tethered Child Spacecraft The actuated scheme shown in Figure 5 uses thrusters on the child spacecraft to move it to the desired location on the target spacecraft, with the tether unreeling speed equaling the child spacecraft speed to keep the tether taut. The child spacecraft can follow the same glideslope trajectory as the propulsive docking parent spacecraft, though the reduced mass affects the required propellant mass. The required propellant mass for the child spacecraft is 0.22 g. After the child has docked with the target, the parent spacecraft begins reeling in the tether.

Spin-Released Tether In the unactuated scheme (Fig 6), the parent spacecraft spins up which deploys the tether using centrifugal force, then the child spacecraft is captured using a retractable arm on the target. This strategy simplifies the child and parent spacecrafts because the child spacecraft

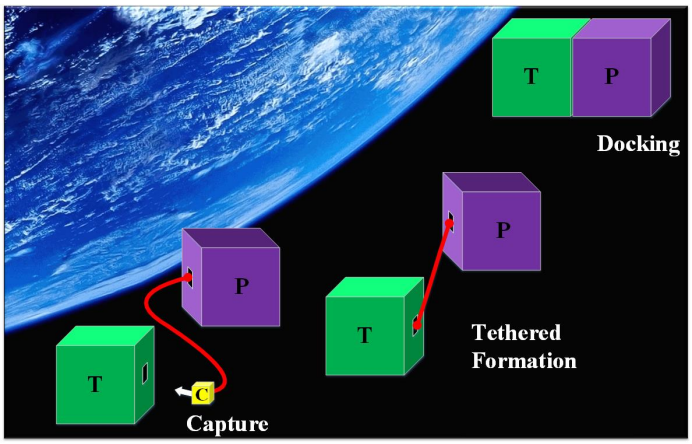

Figure 5. Free-flying child tether-based capture and docking scenario

does not need propulsion, but it complicates the target spacecraft because it requires a retractable arm to capture the child spacecraft. Once the spacecraft are connected with the tether, the tether attributes can be leveraged to aide in relative positioning.

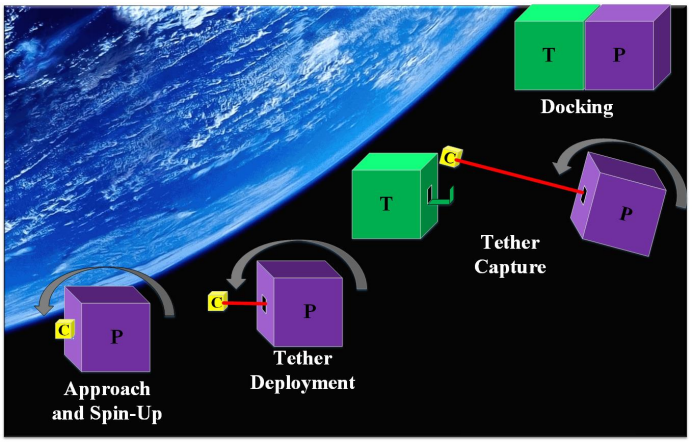

Figure 6. Spinning tether-based capture and docking scenario

CubeSat attitude determination and control is actually fairly advanced. The Blue Canyon Technologies XACT system claims attitude control within 0.003°.[19,20] XACT can also sustain a slew rate of 10°/s. This slew rate was used to saturate the controller during spin-up. The controller used here is a simple proportional controller acting on the torque about the parent body Y axis.

$$\tau_Y = K_P \| r_{child} - r_{child_f} \| \tag{14}$$

Tether Reeling

Once the target and parent are connected by a tether, the tether motor in the parent spacecraft can reel in the target spacecraft without the use of propellant. This causes complex pendulum modes to form in the dumbbell-type system, but these modes can be controlled using only the reaction

wheel assembly in both agents. Controlling these modes does require the cooperation of the target spacecraft.[13,14]

CONCLUSION

Tether-based docking shows a reduction in required fuel mass for the proposed berthing-type mission. Though the savings in fuel is small enough that the added hardware complexity easily outweighs it, the reduction in risk associated with docking is quite substantial. Tether-based docking is advantageous for multi-agent docking missions because it allows multiple satellites to dock simultaneously with minimal docking-based perturbations. Multi-agent docking missions relying on hundreds or thousands of successful docks for mission success and tether-based docking makes this more attainable.

ACKNOWLEDGMENTS

This work was supported by a NASA Space Technology Research Fellowship. Government sponsorship is acknowledged. This research was carried out in part at the Jet Propulsion Laboratory, California Institute of Technology, under a contract with the NASA.

REFERENCES

[1] J. Bonometti, "Boom rendezvous alternative docking approach," *Space*, 2006, pp. 19–21.

[2] "Overview of the DART Mishap Investigation Results," `https://www.nasa.gov/pdf/148072main_DART_mishap_overview.pdf`. Accessed: 2016-12-11.

[3] S. Bandyopadhyay, R. Foust, G. P. Subramanian, S.-J. Chung, and F. Y. Hadaegh, "Review of Formation Flying and Constellation Missions Using Nanosatellites," *Journal of Spacecraft and Rockets*, No. 0, 2016, pp. 567–578.

[4] G. Bonin, N. Roth, S. Armitage, J. Newman, B. Risi, and R. E. Zee, "CanX–4 and CanX–5 Precision Formation Flight: Mission Accomplished!," 2015.

[5] W. Fehse, *Automated rendezvous and docking of spacecraft*, Vol. 16. Cambridge university press, 2003.

[6] J. Mitchell, A. Johnston, R. Howard, M. Williamson, L. Brewster, D. Strack, and S. Cryan, "Automated rendezvous and docking sensor testing at the flight robotics laboratory," 2007.

[7] S.-J. Chung, J.-J. E. Slotine, and D. W. Miller, "Nonlinear model reduction and decentralized control of tethered formation flight," *Journal of Guidance, Control, and Dynamics*, Vol. 30, No. 2, 2007, pp. 390–400.

[8] S.-J. Chung, *Nonlinear control and synchronization of multiple Lagrangian systems with application to tethered formation flight spacecraft*. PhD thesis, Massachusetts Institute of Technology, 2007.

[9] O. Mori and S. Matunaga, "Formation and attitude control for rotational tethered satellite clusters," *Journal of Spacecraft and Rockets*, Vol. 44, No. 1, 2007, pp. 211–220.

[10] M. Nohmi, "Mission design of a tethered robot satellite STARS for orbital experiment," *Control Applications,(CCA) & Intelligent Control,(ISIC), 2009 IEEE*, IEEE, 2009, pp. 1075–1080.

[11] M. Duzzi, L. Olivieri, and A. Francesconi, "Tether-aided spacecraft docking procedure," 4S Symposium, 2016.

[12] D. Petrillo, M. Buonomo, A. Cavinato, F. Chiariotti, M. Gaino, F. Branz, R. Mantellato, L. Olivieri, F. Sansone, A. Francesconi, *et al.*, "Flexible Electromagnetic Leash Docking system (FELDs) experiment from design to microgravity testing," *66Th International Astronautical Congress, IAC-15 E*, Vol. 2, 2015.

[13] S.-J. Chung and D. W. Miller, "Propellant-free control of tethered formation flight, part 1: Linear control and experimentation," *Journal of guidance, control, and dynamics*, Vol. 31, No. 3, 2008, pp. 571–584.

[14] S.-J. Chung, J.-J. E. Slotine, and D. W. Miller, "Propellant-free control of tethered formation flight, part 2: Nonlinear underactuated control," *Journal of guidance, control, and dynamics*, Vol. 31, No. 5, 2008, pp. 1437–1446.

[15] "Propulsion Unit for CubeSats," `http://www.vacco.com/images/uploads/pdfs/11044000-01_PUC.pdf`. Accessed: 2017-4-11.

[16] Y. Ariba, D. Arzelier, L. S. Urbina, and C. Louembet, "V-bar and R-bar Glideslope Guidance Algorithms for Fixed-Time Rendezvous: A Linear Programming Approach," *IFAC-PapersOnLine*, Vol. 49, No. 17, 2016, pp. 385–390.

[17] H. B. Hablani, M. L. Tapper, and D. J. Dana-Bashian, "Guidance and relative navigation for autonomous rendezvous in a circular orbit," *Journal of Guidance, Control, and Dynamics*, Vol. 25, No. 3, 2002, pp. 553–562.

[18] H. D. Curtis, *Orbital mechanics for engineering students*. Butterworth-Heinemann, 2013.

[19] "Attitude Determination Control Systems," `http://bluecanyontech.com/wp-content/uploads/2017/04/DataSheet_ADCS_07_F.pdf`. Accessed: 2017-5-11.

[20] G. P. Subramanian, R. Foust, D. Chen, S. Chan, Y. Taleb, D. L. Rogers, J. Kokkat, S. Bandyopadhyay, D. Morgan, S.-J. Chung, *et al.*, "Information-driven systems engineering study of a formation flying demonstration mission using six CubeSats," *53rd AIAA Aerospace Sciences Meeting*, 2015, p. 2043.